Steel and Composite Structures, *Vol. 17, No. 5 (2014) 667-686*
DOI: http://dx.doi.org/10.12989/scs.2014.17.5.667

Experiments on the bearing capacity of tapered concrete filled double skin steel tubular (CFDST) stub columns

Qing-Xin Ren [1,2a], Chao Hou [2b], Dennis Lam [3c] and Lin-Hai Han [*2]

[1] *School of Civil Engineering, Shenyang Jianzhu University, Shenyang 110168, PR China*
[2] *Department of Civil Engineering, Tsinghua University, Beijing 100084, PR China*
[3] *School of Engineering, University of Bradford, Bradford BD7 1DP, UK*

(*Received November 17, 2013, Revised March 24, 2014, Accepted April 06, 2014*)

Abstract. Tapered concrete filled double skin steel tubular (CFDST) columns have been used in China for structures such as electricity transmission towers. In practice, the bearing capacity related to the connection details on the top of the column is not fully understood. In this paper, the experimental behaviour of tapered CFDST stub columns subjected to axial partial compression is reported, sixteen specimens with top endplate and ten specimens without top endplate were tested. The test parameters included: (1) tapered angle, (2) top endplate thickness, and (3) partial compression area ratio. Test results show that the tapered CFDST stub columns under axial partial compression behaved in a ductile manner. The axial partial compressive behaviour and the failure modes of the tapered CFDST stub columns were significantly influenced by the parameters investigated. Finally, a simple formula for predicting the cross-sectional capacity of the tapered CFDST sections under axial partial compression is proposed.

Keywords: concrete filled steel tube (CFST); concrete filled double skin steel tube (CFDST); tapered column; axial partial compression; cross-sectional capacity

1. Introduction

In the past ten years, much attention has been paid towards the concrete filled double skin steel tubular (CFDST) members consisting of outer and inner steel with concrete filled in between (Zhao and Han 2006). These members inherit advantages from conventional concrete filled steel tubes (CFST) and are characterized by a smaller self-weight and better cyclic performance due to two layers of steel tubes. A lot of studies have been carried out on CFDST members with a uniform cross-section along the longitudinal direction (referred as "straight member" in this paper), such as Zhao *et al*. 2002, 2010, Tao *et al*. 2004, Uenaka *et al*. 2008, Hu and Su 2011, Dong and Ho 2012, Kim *et al*. 2013 and Shimizu *et al*. 2013.

In recent years, tapered members with cross-section varied along the longitudinal direction

*Corresponding author, Professor, E-mail: lhhan@tsinghua.edu.cn
[a] Associate Professor
[b] Post-Doctoral Fellow
[c] Professor

http://www.techno-press.org/?journal=scs&subpage=8 ISSN: 1229-9367 (Print), 1598-6233 (Online)

have been adopted for architecture reasons, moreover, this has also become an economical choice in some cases when compared with the parallel sections. The behaviour of tapered concrete filled steel tubular (CFST) columns and tapered concrete filled double skin steel tubular (CFDST) columns under entirely compression have been studied extensively over the last few years. Han *et al*. (2010) studied the experimental behaviour of the tapered CFST stub columns. A parametric study into the behaviour of the tapered CFST stub columns was conducted by Lam *et al*. (2012). Han *et al*. (2011) carried out experiments on the behaviour of axially loaded tapered stainless steel–concrete–carbon steel double skin tubular stub columns. Li *et al*. (2012) conducted experimental investigations of axial loaded tapered CFDST stub columns and developed a finite element analysis (FEA) model to predict their behaviour. Li *et al*. (2013) reported investigations on eccentrically loaded tapered CFDST columns with different eccentricities and used the finite element model to predict the behaviour of the tapered member.

Tapered CFDST columns have been used for electricity transmitting poles due to the advantages of CFDST column over traditional CFST column (Li *et al*. 2012, 2013), it could also be used as bridge piers over deep valleys and bearing members of rigid frame or reticulate frame. However, the bearing details for this form of composite columns are not fully understood, thick endplate is usually used to transfer the load directly to the column and to ensure that full compression onto the steel and concrete is achieved.

The behaviour of CFST columns under partial compression has been extensively studied by some researchers in recent years. Han *et al*. (2008) experimentally investigated the behaviour of CFST stub columns subjected to axially local compression. Yang and Han (2012) studied the behaviour of thin-walled CFST column subjected to concentric partial compression. The experimental behaviour of CFDST sections subjected to partial compression is reported by Yang *et al*. (2012). However, it seems that there is no information available for the behaviour of tapered CFDST columns under partial compression. It is expected that the mechanism of tapered CFDST columns under partial compression is different from that of the straight members due to the tapered angle.

A series of tests were conducted on tapered CFDST stub columns under axial partial compression, a total of 26 specimens were tested, 16 specimens with top endplate and 10 specimens without top endplate. The test parameters included the tapered angle, the top endplate thickness and the partial compression area ratio. The main objectives of this research work presented are threefold. Firstly, to report a series of test results of tapered CFDST stub columns under axial partial compression. Secondly, to study the influence of the tapered angle, the top endplate thickness and the partial compression area ratio on the composite columns and thirdly, to develop an evaluation method that could be used to predict the cross-sectional capacity of tapered CFDST stub columns under axial partial compression.

2. Experimental investigations

2.1 Test specimens

26 tapered CFDST stub column tests were carried out, including 16 specimens with top endplate and 10 specimens without top endplate. All specimens are with outer and inner tubes of circular section.

Fig. 1 illustrates the tapered CFDST stub columns under axial partial compression. The information of the testing specimens are listed in Table 1, where D (d) is the outside diameter of

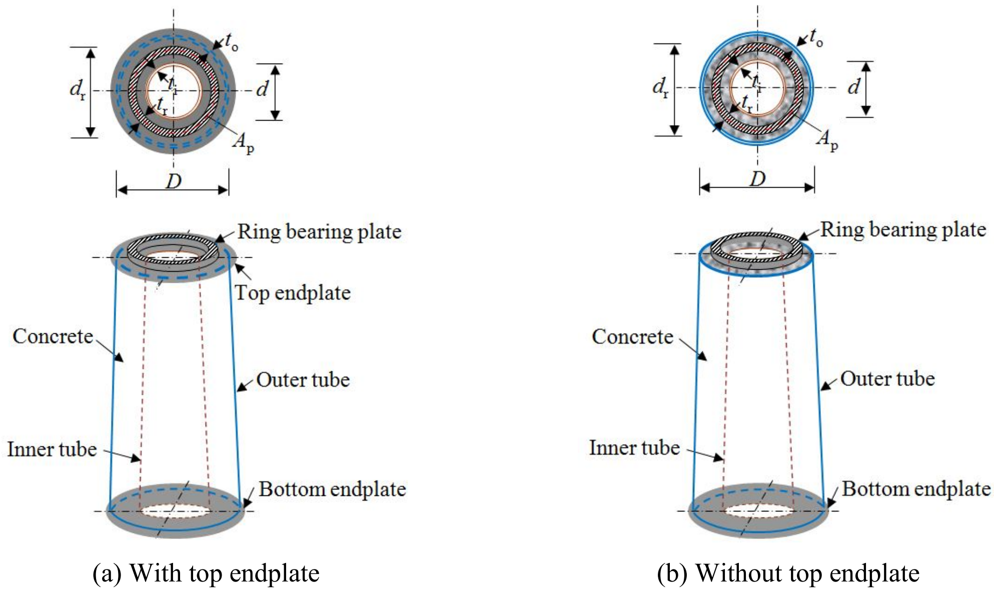

Fig. 1 Tapered CFDST stub columns under axial partial compression

of outer (inner) circular steel tube; t_o (t_i) is the wall thickness of the outer (inner) steel tube.

Circular steel rings were used as the bearing plates for tapered CFDST stub columns, and the central line of the ring is coincided with the central line of the sandwich concrete, as shown in Fig. 1. In Fig. 1, d_r is the outside diameter of the ring bearing plate, and t_r is the wall thickness of the ring bearing plate. The height of the ring bearing plate used is 80 mm for all the tests.

Based on the references of existing tapered structural columns, The test parameters for the tapered CFDST stub columns under axial partial compression include:

(1) Tapered angle (θ): 0°, 0.57° and 1.14°.
(2) Top endplate thickness (t_a): 4 mm, 12 mm and 20 mm.
(3) Partial compression area ratio (β): 2, 4 and 6.

The partial compression area ratio (β) is defined as

$$\beta = \frac{A_c}{A_p} \tag{1}$$

where, A_c is the cross-sectional area of the sandwich concrete at the top section, and A_p is the partial bearing area of the compressive load, i.e. the cross-sectional area of the ring bearing plate.

The following notations are used to characterize each specimen.

- The initial character "p" stands for the axial partial compression;
- The following character "c" stands for the stub column specimens;
- The third character "p" (if used) stands for the top endplate;
- The last character "h" (if used) stands for the hollow section without filling sandwich concrete;
- The first number represents the groups of the same stub column specimens type, and the second number represents the different specimen in the same group.

For example, the specimen with the label "pcph1-2" denotes the second specimen in the first group of the tapered stub columns with top endplate under axial partial compression, where hollow section is used, i.e., unfilled.

The tubes were all manufactured from mild steel plates, the specified sectional shape was cut from the plates, cold rolled and welded into a circular section with a single bevel butt weld. Before pouring the concrete, inner and outer hollow tubes were welded to a 20 mm thick steel baseplate at one end.

Two types of steel were used to manufacture the outer and inner tubes. Standard tensile coupon tests were conducted to evaluate the tensile strength of the steel tubes. The measured average of the wall thickness (t), yield strength (f_y), ultimate strength (f_u), modulus of elasticity (E_s) and Poisson's ratio (γ_s) are given in Table 2.

Table 1 Information of the testing specimens

Specimen type	No.	Specimen number	Outer tube $D \times t_o$ (mm)		Inner tube $d \times t_i$ (mm)		H (mm)	θ (°)	t_a (mm)	β	N_{ue} (kN)		SI
			Top section	Bottom section	Top section	Bottom section					Measure	Average	
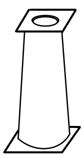	1	pcp1-1	350×3.82	350×3.82	231×2.92	231×2.92	1050	0	12	4	4288	4266	1.005
	2	pcp1-2	350×3.82	350×3.82	231×2.92	231×2.92	1050	0	12	4	4244		0.995
	3	pcp2-1	329×3.82	350×3.82	210×2.92	231×2.92	1050	0.57	12	4	3980	3996	0.933
	4	pcp2-2	329×3.82	350×3.82	210×2.92	231×2.92	1050	0.57	12	4	4011		0.940
	5	pcp3-1	308×3.82	350×3.82	189×2.92	231×2.92	1050	1.14	12	4	3821	3829	0.896
	6	pcp3-2	308×3.82	350×3.82	189×2.92	231×2.92	1050	1.14	12	4	3837		0.899
	7	pcp4-1	329×3.82	350×3.82	210×2.92	231×2.92	1050	0.57	4	4	3027	3060	0.710
	8	pcp4-2	329×3.82	350×3.82	210×2.92	231×2.92	1050	0.57	4	4	3092		0.725
	9	pcp5-1	329×3.82	350×3.82	210×2.92	231×2.92	1050	0.57	20	4	4947	4919	1.160
	10	pcp5-2	329×3.82	350×3.82	210×2.92	231×2.92	1050	0.57	20	4	4891		1.147
	11	pcp6-1	329×3.82	350×3.82	210×2.92	231×2.92	1050	0.57	12	2	4489	4551	1.052
	12	pcp6-2	329×3.82	350×3.82	210×2.92	231×2.92	1050	0.57	12	2	4613		1.081
	13	pcp7-1	329×3.82	350×3.82	210×2.92	231×2.92	1050	0.57	12	6	3707	3805	0.869
	14	pcp7-2	329×3.82	350×3.82	210×2.92	231×2.92	1050	0.57	12	6	3903		0.915
	15	pcph1-1	329×3.82	350×3.82	210×2.92	231×2.92	1050	0.57	12	4	1672	1595	0.392
	16	pcph1-2	329×3.82	350×3.82	210×2.92	231×2.92	1050	0.57	12	4	1518		0.356
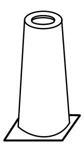	17	pc1-1	350×3.82	350×3.82	231×2.92	231×2.92	1050	0	-	4	2093	2096	0.999
	18	pc1-2	350×3.82	350×3.82	231×2.92	231×2.92	1050	0	-	4	2099		1.001
	19	pc2-1	329×3.82	350×3.82	210×2.92	231×2.92	1050	0.57	-	4	2088	2089	0.996
	20	pc2-2	329×3.82	350×3.82	210×2.92	231×2.92	1050	0.57	-	4	2090		0.997
	21	pc3-1	308×3.82	350×3.82	189×2.92	231×2.92	1050	1.14	-	4	2086	2085	0.995
	22	pc3-2	308×3.82	350×3.82	189×2.92	231×2.92	1050	1.14	-	4	2084		0.994
	23	pc4-1	329×3.82	350×3.82	210×2.92	231×2.92	1050	0.57	-	2	3274	3212	1.562
	24	pc4-2	329×3.82	350×3.82	210×2.92	231×2.92	1050	0.57	-	2	3149		1.502
	25	pc5-1	329×3.82	350×3.82	210×2.92	231×2.92	1050	0.57	-	6	1596	1592	0.761
	26	pc5-2	329×3.82	350×3.82	210×2.92	231×2.92	1050	0.57	-	6	1588		0.758

Table 2 Material properties of steel

Type	t (mm)	f_y (MPa)	f_u (MPa)	E_s (GPa)	γ_s
Inner tube	2.92	396.5	530.7	202	0.295
Outer tube	3.82	439.3	508.5	212	0.307

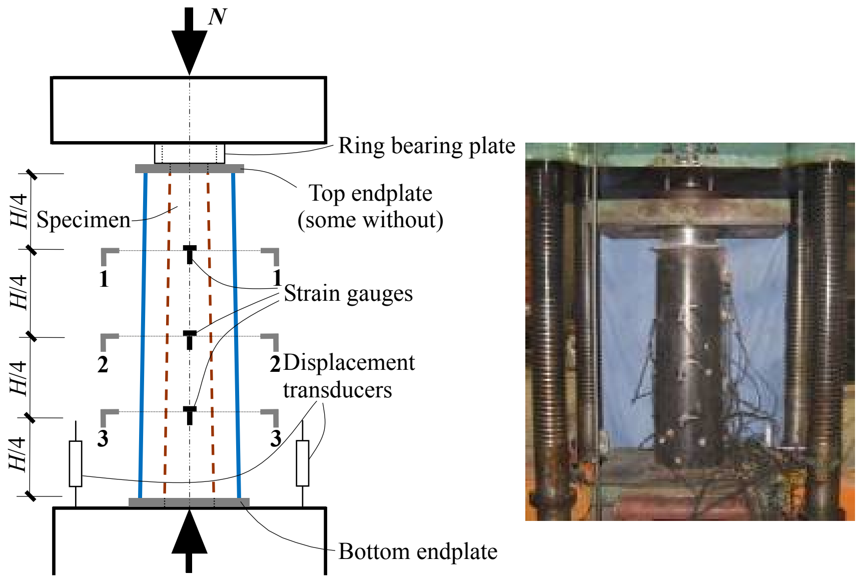

Fig. 2 Test setup of tapered CFDST stub columns

Self-consolidating concrete (SCC) was poured into the space between the outer and inner tube without any vibration, then the specimens were placed upright until the test. The SCC mixture was designed with a compressive cube strength (f_{cu}) at 28 days of approximately 50 MPa. The mix proportions are: cement: 385 kg/m^3, blast furnace slag: 165 kg/m^3, water: 190 kg/m^3, sand: 785 kg/m^3, coarse aggregate: 850 kg/m^3, and additional high-range water reducer (HRWR): 5.5kg/m^3.

In the concrete mixes, silica-based sand was used as the fine aggregate whilst carbonate stone was used as the coarse aggregate. The compressive cube strength and elastic modulus of concrete were obtained by testing 150 mm cubes and $150 \times 150 \times 300$ mm prisms, respectively. The average cube strength (f_{cu}) at 28 days and at the time of testing were 48.6 and 52.2 MPa respectively. The modulus of elasticity (E_c) of concrete at 28 days was 33 GPa. The measured slump and spreading of the fresh SCC were 270 mm and 674 mm respectively.

During the curing of the sandwich concrete, a very small amount of longitudinal shrinkage was observed at the top of the specimen. A high strength grouting material was then used to fill this gap so that the concrete surface was flush with the outer and inner steel tubes at the top. Finally an annular steel cover plate was welded to the outer and inner steel tubes of the specimens with top endplate in order to transfer the load to the composite section.

2.2 Test setup

Fig. 2 shows the schematics diagram and photos of the test setup. A universal test machine with the compressive capacity of 5,000 kN was used for all the tests, the compressive loads were applied on the ring bearing plate through the loading ram of the test machine.

To obtain the longitudinal and transverse strains of the outer and inner steel tube, three sections denoted by numbers 1, 2 and 3 were selected to position the strain gauges (four longitudinal strain gauges and four transverse strain gauges are installed per section) and the strain gauges were located at the outer surface of the outer and inner steel tube. Before the inner steel tubes were welded to the bottom endplate, the strain gauges located at the outer surface of the inner steel tube were protected with epoxy adhesive. For all specimens, there are strain gauges at Sections 1 to 3 of the outer tube and Section 2 of the inner tube. Two displacement transducers were used to measure the axial deformations as shown in Fig. 2.

Load increments of about one tenth of the estimated cross-sectional capacity were applied. Each load increment was maintained for approximately 2 min. The unloading stage of each specimen was also recorded and generally the loading was terminated when the axial deformation have reached height /35 (30 mm).

2.3 Test results

It was found that all tapered CFDST specimens behaved in a ductile manner. Figs. 3 and 4 show the photos of the tested specimens with and without top endplate. Fig. 5 gives the typical failure modes of the tapered CFDST and double skin steel tubular stub columns, Fig. 6 demonstrates the typical failure modes of the inner steel tube, and Fig. 7 illustrates the typical exposed views of the sandwich concrete.

It can be seen from Figs. 3 and 5(a) that for tapered CFDST stub columns with top endplate, there was a U-shape ring-like impression at the top surface of the top endplate and the top endplate showed an upward deformation near the corners and sunken in the middle, the "parachute" like shape of the top endplate is owing to the concrete crushed under the ring bearing plate. The

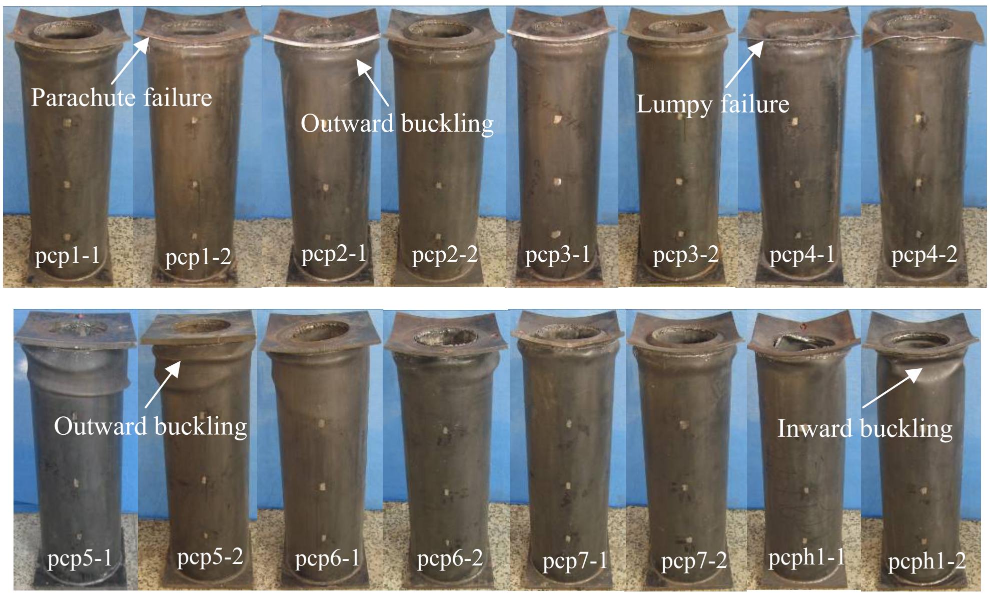

Fig. 3 Failure modes of the tested specimens with top endplate

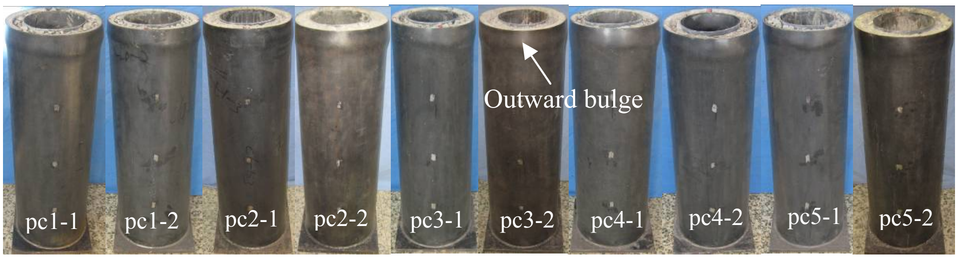

Fig. 4 Failure modes of the tested specimens without top endplate

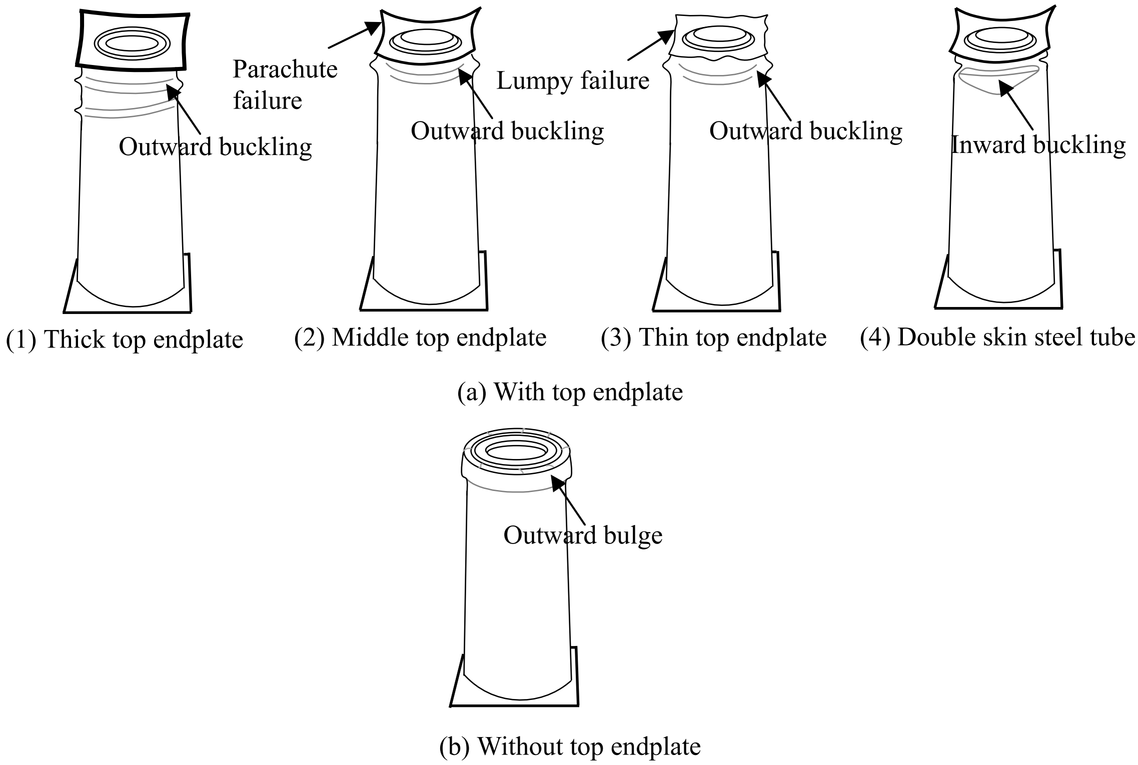

Fig. 5 Typical failure modes of tapered CFDST and double skin steel tubular stub columns

outward deformation of the outer steel tube and the inward deformation of the inner steel tube (see Fig. 6(a)) occur at the section near the top endplate due to the local crushing effect of the infill concrete. In general, the tapered angle (θ) has moderate effect on the failure modes of the specimens with top endplate, whereas the top endplate thickness (t_a) and the partial compression area ratio (β) have significant influence to the behaviour. The larger the top end plate thickness and the lower the partial compression area ratio, the larger is the plastic deformation range. This is due to the fact that the load transfer area becomes larger with the thicker endplate and the smaller partial compression area ratio. It can be seen in Fig. 7(a) that the infill sandwich concrete was crushed where the outward buckling was formed. The outer and inner tubes of the hollow double skin steel tubular specimens behaved differently from those of the concrete filled columns. For the

(a) With top endplate (b) Without top endplate

Fig. 6 Failure modes of the inner steel tube

(a) With top endplate (b) Without top endplate

Fig. 7 Failure modes of the sandwich concrete

hollow double skin steel tubular stub columns, the outward and inward local buckling was observed on the top of the column, as shown in Fig. 3.

Tapered CFDST stub columns without top endplate is shown in Figs. 4, 5(b) and 6(b), there is radial bulgy for outer steel tubes and contractive plastic deformation for inner steel tubes. This may be explained by that when subjected to axial partial compression, the steel tubes of tapered CFDST specimens without top endplate do not directly undertake the axial loads, and the concrete on both sides of the bearing plate deforms laterally owing to the compression of the bearing plate. In general, the tapered angle (θ) and the partial compression area ratio (β) have moderate effect on the failure modes of the specimens without top endplate. As shown in Fig. 7(b), for the tapered CFDST stub columns without top endplate, the infill sandwich concrete was fully cracked near the top.

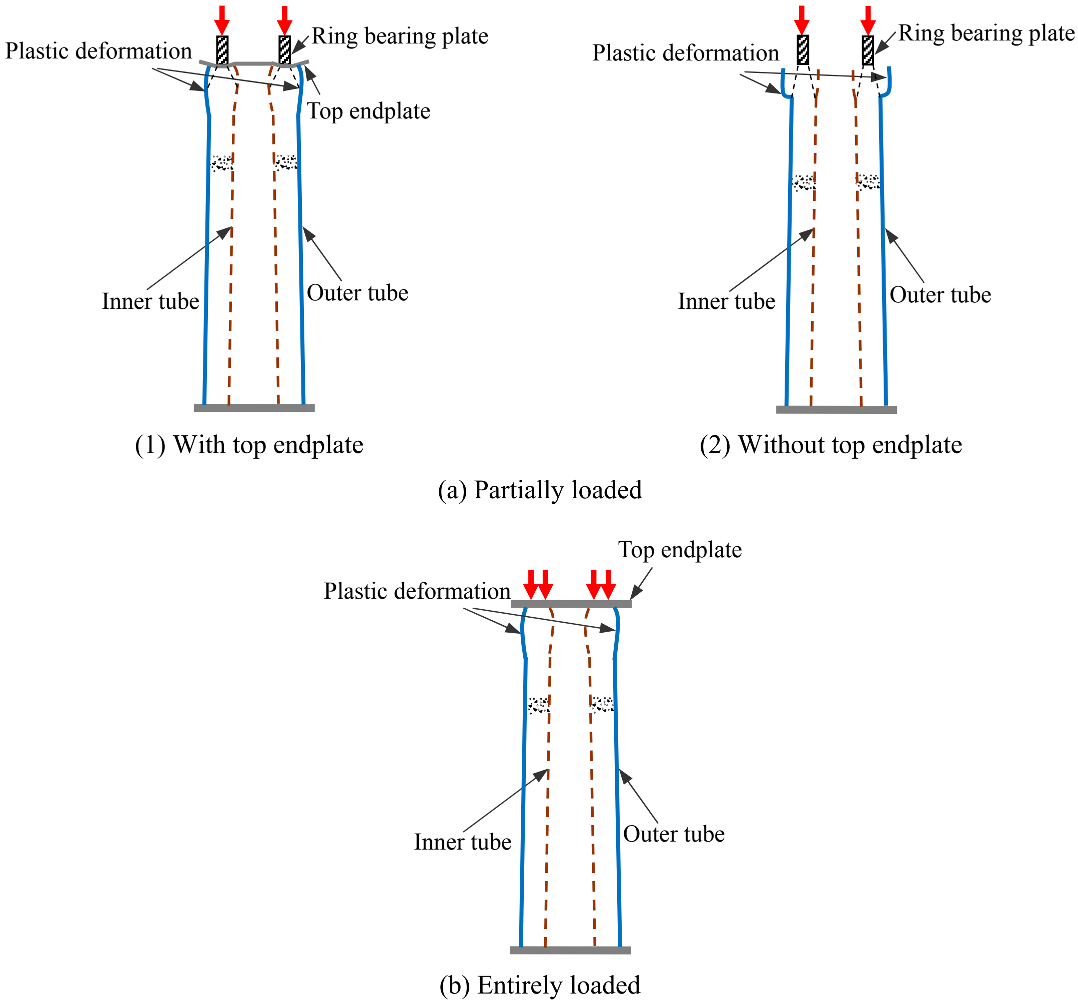

Fig. 8 Typical load transfer paths of partially and entirely loaded tapered CFDST specimens

Fig. 8 illustrates the typical load transfer paths of partially and entirely loaded tapered CFDST specimens. It can be found that for partially loaded tapered CFDST columns, the load transfers down like an isosceles trapezoid, which is different from those of the entirely loaded tapered CFDST columns. It can also be observed that the failure position is generally located on the top part of partially loaded tapered CFDST columns, which is similar to those of the entirely loaded tapered CFDST columns (Han *et al*. 2010, 2011, Li *et al*. 2012) and the partially loaded CFDST columns (Yang *et al*. 2012).

Figs. 9 and 10 show the measured axial load (N) versus axial deformation (Δ) relationship of the tested specimens with and without top endplate. The bearing capacity (N_{ue}) (i.e., the first peak load) of the specimens is given in Table 1. It can be observed that the N-Δ curve of the specimens with top endplate regained some of the bearing capacity after the first peak load at a deformation of around 1.5% of the column height (15 mm). This is different to the behaviour observed from tests when the column were entirely loaded where no strength enhancement was observed after the

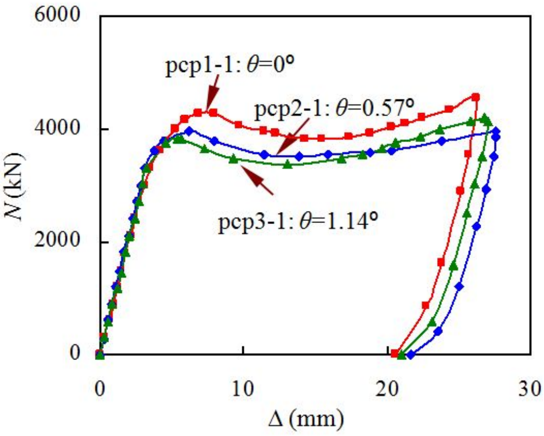

(a) Tapered angle

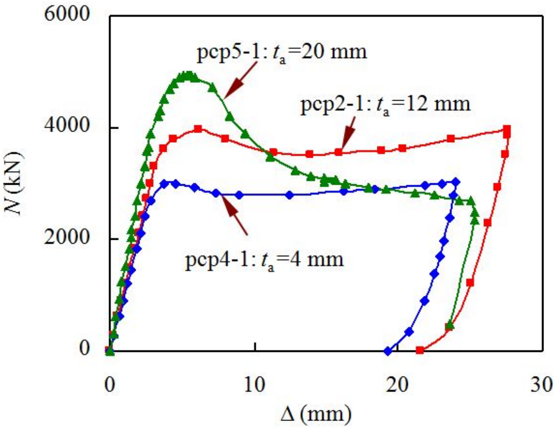

(b) Top endplate thickness

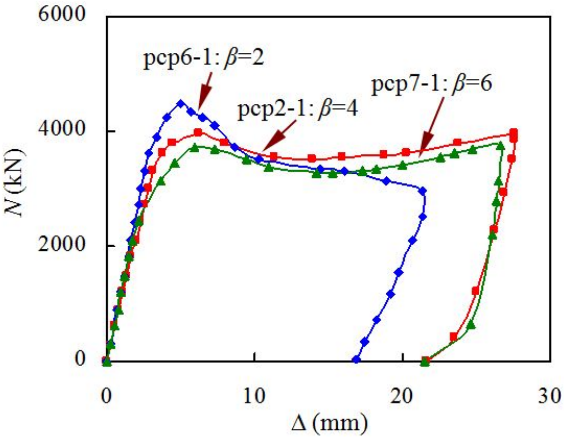

(c) Partial compression area ratio

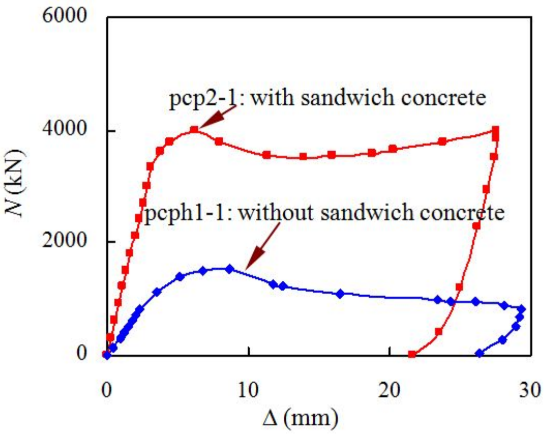

(d) With or without sandwich concrete

Fig. 9 Measured axial load (N) versus deformation (Δ) relationship of sepcimens with top endplate

peak load. The comparison of the different bearing conditions is shown in Fig. 11.

With regarding to the tapered angle (θ), it has moderate effects on the N-Δ curve of the specimens with top endplate, whereas the top endplate thickness (t_a), the partial compression area ratio (β) and the infill sandwich concrete have significant effects on the specimens with top endplate. The initial slope of N-Δ curve and the bearing capacity of partially loaded tapered CFDST columns decrease slightly with the increase of the tapered angle (θ). This can be explained by that the tapered CFDST specimen with a bigger tapered angle has a smaller cross-sectional area on the top section and hence a reduction in its bearing capacity. Furthermore, similar to the results of partially loaded CFDST columns reported by Yang *et al*. 2012, the thinner of the top endplate thickness (t_a) together with the higher partial compression area ratio (β), led to a lower initial stiffness and bearing capacity. This is due to the fact that with the high partial compression area ratio, high concentrated bearing stress is applied to the small section of concrete directly beneath the bearing plate and hence the reduction in strength. The thicker endplate has a higher flexural rigidity under axial loading and led to higher bearing capacity, however with little regaining in

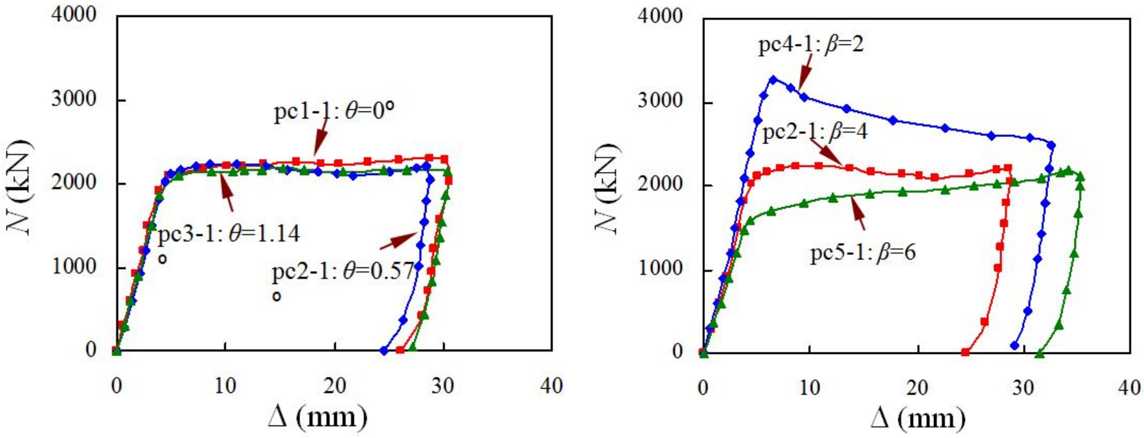

(a) Tapered angle (b) Partial compression area ratio

Fig. 10 Measured axial load (N) versus deformation (Δ) relationship of sepcimens without top endplate

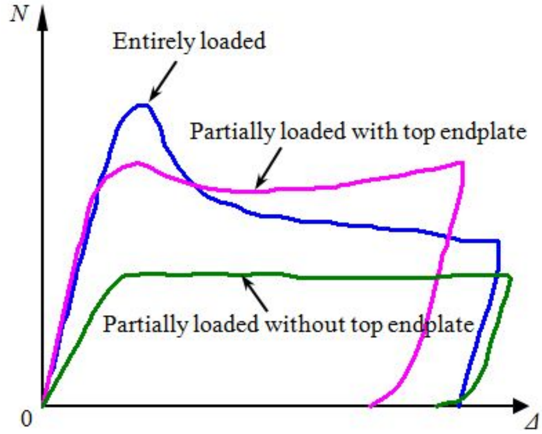

Fig. 11 Typical axial load (N) versus deformation (Δ) relationship for tapered CFDST stub columns

strength after the first peak load.

It can be observed from Fig. 10 that the tapered angle (θ) has little effect on the N-Δ curve of the specimens without top endplate, whereas the partial compression area ratio (β) has significant effects on those specimens without top endplate, which is the same as that of the specimens with top endplate.

Figs. 12 and 13 show the load (N) versus strain (ε) relationship at different sections for the inner and outer tubes along the length of the column (see Fig. 2), where the longitudinal and transverse strains are marked by small letter 'l' and 't' in the subscript respectively. The tensile strain are denoted as negative while compressive strain as positive, and ε_{yo} and ε_{yi} are the yield strain of outer and inner steel tube respectively. It can be observed from both outer and inner steel tube that the strain values at Section 1 is generally higher than that at Sections 2 and 3 owing to the concentration of the plastic deformations of the steel tubes near the top of the specimen. The strain of the outer steel tube is larger than that of the inner steel tube. This can be explained by that the

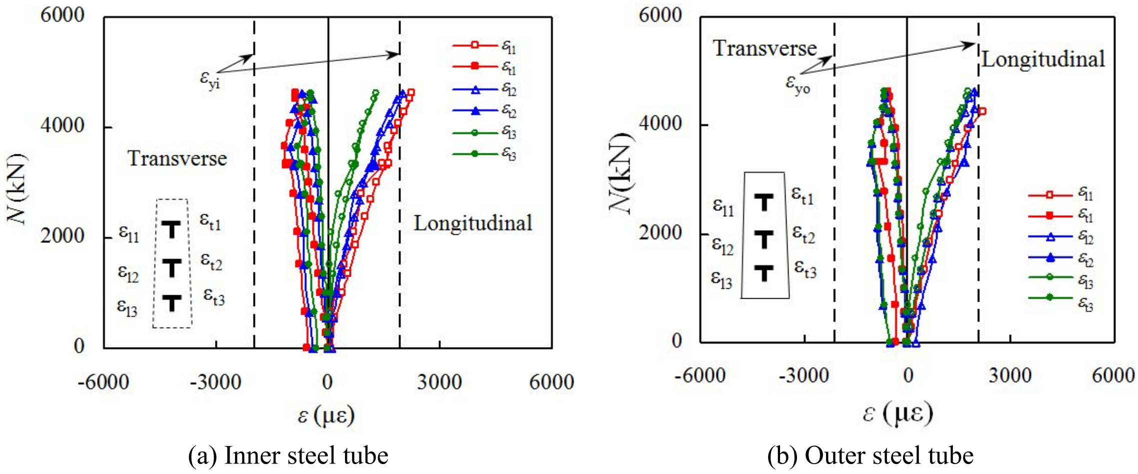

Fig. 12 Typical axial load (N) versus strain (ε) relationship of sepcimens with top endplate

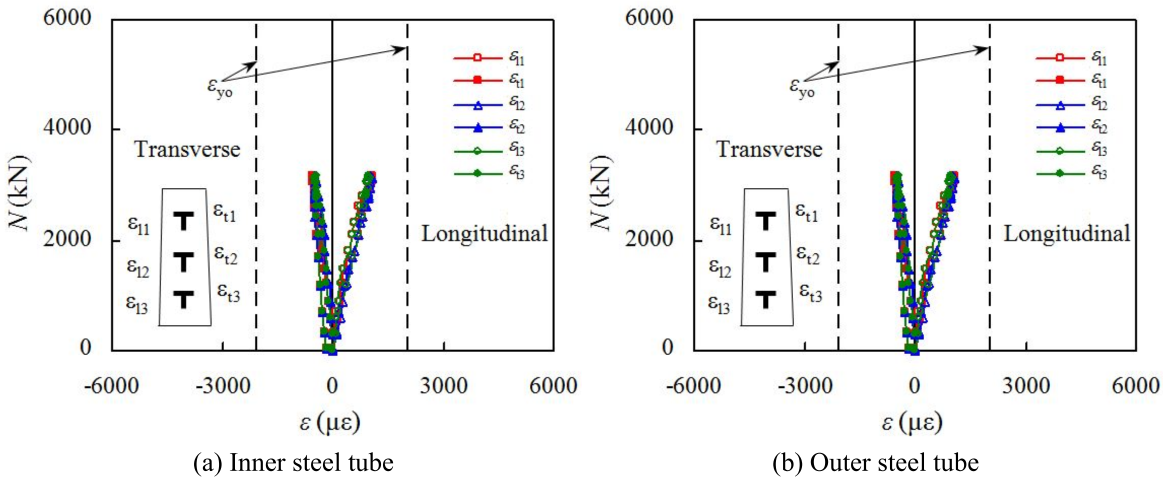

Fig. 13 Typical axial load (N) versus strain (ε) relationship of specimens without top endplate

diameter to thickness ratio of the outer steel tube is larger than that of the inner steel tube and the outer steel tube is prone to local buckling under the same axial deformation when compared with the inner steel tube. It can also be observed that the strain in the steel tubes with top endplate is larger than that of the specimens without top endplate. This is due to the fact that specimens without top endplate generally failed by local crushing failure of the concrete.

3. Analysis and discussions

3.1 Strength Index, SI

For convenience of analysis, a strength index (SI) is defined to quantify the axial partial

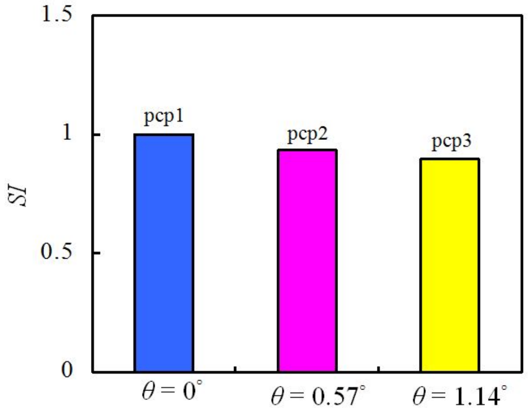

(a) Tapered angle

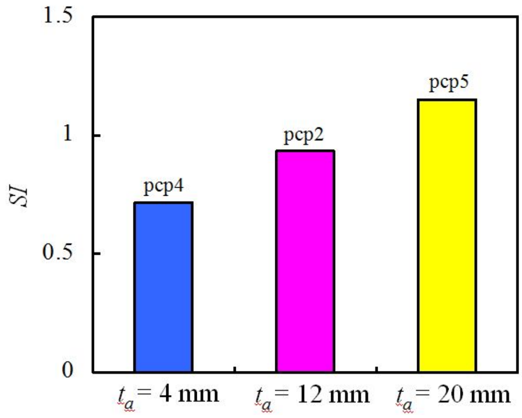

(b) Top endplate thickness

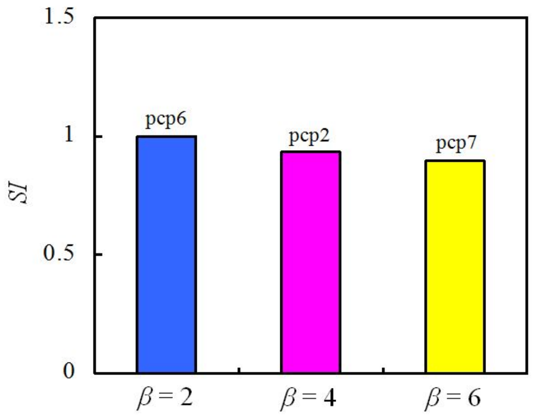

(c) Partial compression area ratio

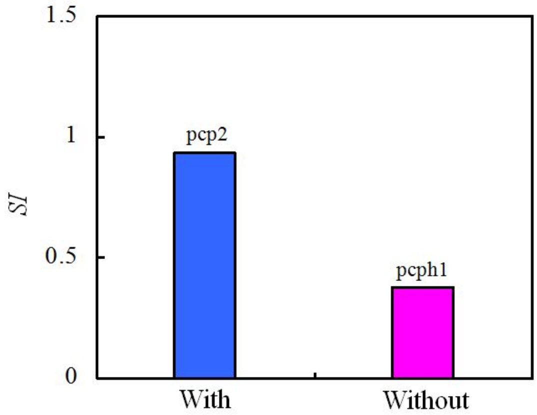

(d) With or without sandwich concrete

Fig. 14 Strength index (*SI*) of specimens with top endplate

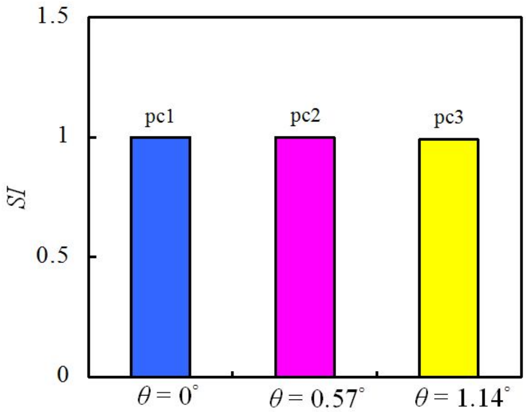

(a) Tapered angle

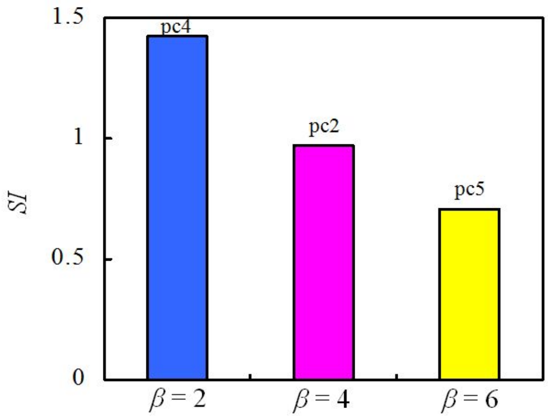

(b) Partial compression area ratio

Fig. 15 Strength index (*SI*) of specimens without top endplate compression bearing capacity as follows

$$SI = \frac{N_{ue}}{N_{ur}} \tag{2}$$

where, N_{ue} is the measured ultimate axial partial compression load; N_{ur} is the average axial partial compression strength of the reference straight CFDST stub columns according to the bottom section. The strength index (SI) for all the specimens are given in Table 1, and plotted for comparison in Figs. 14 and 15 for specimens with and without top endplate.

For tapered CFDST columns with top endplate, SI decreases 6.4% and 10.3% with the increasing of the tapered angle, θ from 0 to 0.57° and to 1.14°. SI increases by 30.5% and 60.8% with the increasing of t_a from 4 mm to 12 mm and to 20 mm. SI decreases by 12.2% and 16.4% with the increasing of β from 2 to 4 and to 6. 150.4% increases in the bearing capacity is observed between hollow section and CFDST column. It can be found that, the influence of β, t_a and the sandwich concrete on the strength index (SI) for the tapered CFDST columns with top endplate is significant, which is consistent with that of the straight CFDST columns. Meanwhile, the influence of θ on the strength of the tapered CFDST columns are quite considerable, the strength has a decrease of 10.3% when θ = 1.14º. This can be explained by the fact that when the bottom section is constant, the top section is reduced with the increase of the tapered angle θ.

For tapered CFDST columns without top endplate, the reduction of the strength index, SI is given in Fig. 15. SI decreases by 0.4% and 0.6% with the increases of the tapered angle, θ from 0 to 0.57° and to 1.14°. SI decreases by 34.7% and 50.4% with the increasing of β from 2 to 4 and to 6. It seems that the influence of θ on the strength index (SI) of the tapered CFDST columns without top endplate is insignificant when compared with that on the ones with top endplate as the specimens mainly failed by local crushing of concrete.

Figs. 16(a) and (b) show the strength index (SI) versus tapered angle (θ) relations of the composite columns with and without top endplate. According to the measured data, empirical formulas of SI with respect to θ were given and shown in Fig. 16.

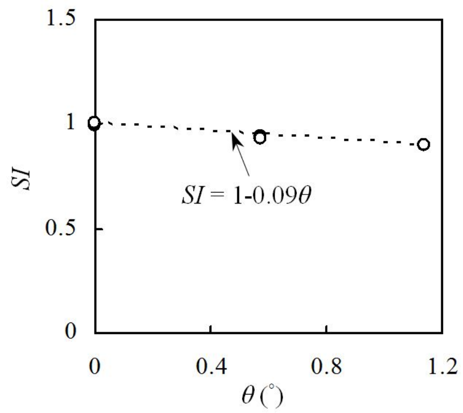

(a) With top endplate

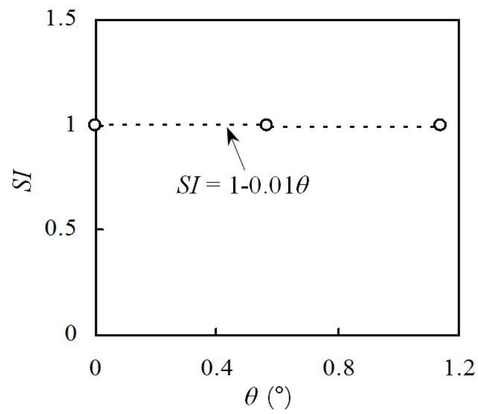

(b) Without top endplate

Fig. 16 Strength index (SI) against tapered angle (θ) curves

3.2 Average strain, $\bar{\varepsilon}_u$

One of the methods used to quantify section ductility is by the average strain. The definition is expressed as follows

$$\bar{\varepsilon}_u = \frac{\Delta_u}{H} \tag{3}$$

where $\bar{\varepsilon}_u$ is the average strain of the testing specimen corresponding to the ultimate load (N_{ue}), Δ_u is the axial displacement corresponding to the ultimate load, and H is the height of the composite column. The average strains $(\bar{\varepsilon}_u)$ for the columns with and without the top endplate are plotted in Figs. 17 and 18.

For the tapered CFDST columns with top endplate, $\bar{\varepsilon}_u$ decreases by 6.4% and 9.1% with the increasing of θ from 0 to 0.57° and to 1.14°. $\bar{\varepsilon}_u$ increases by 22.3% and 16.4% with the increases of t_a from 4 mm to 12 mm and to 20 mm. $\bar{\varepsilon}_u$ increases by 15.7% and 10.5% with the increases

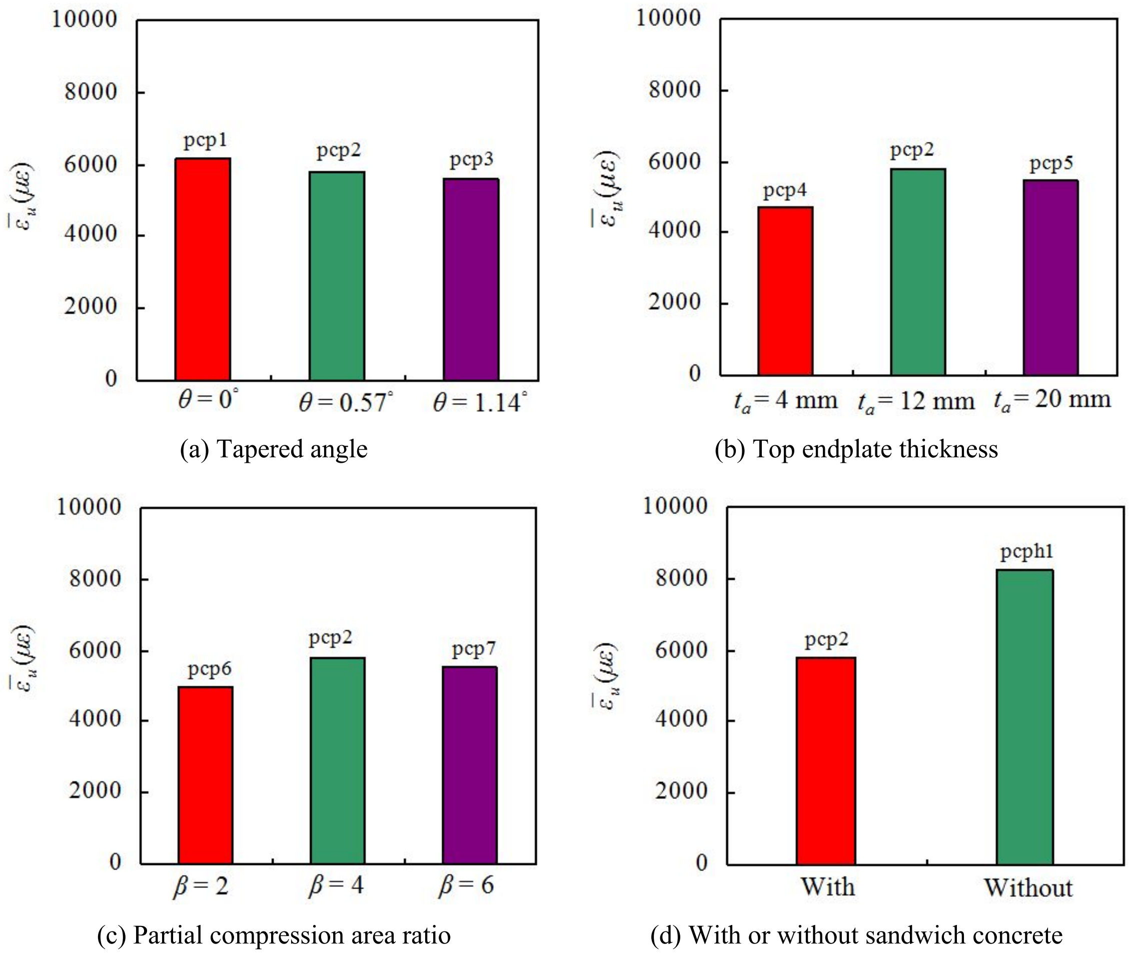

Fig. 17 average strain ($\bar{\varepsilon}_u$) of specimens with top endplate

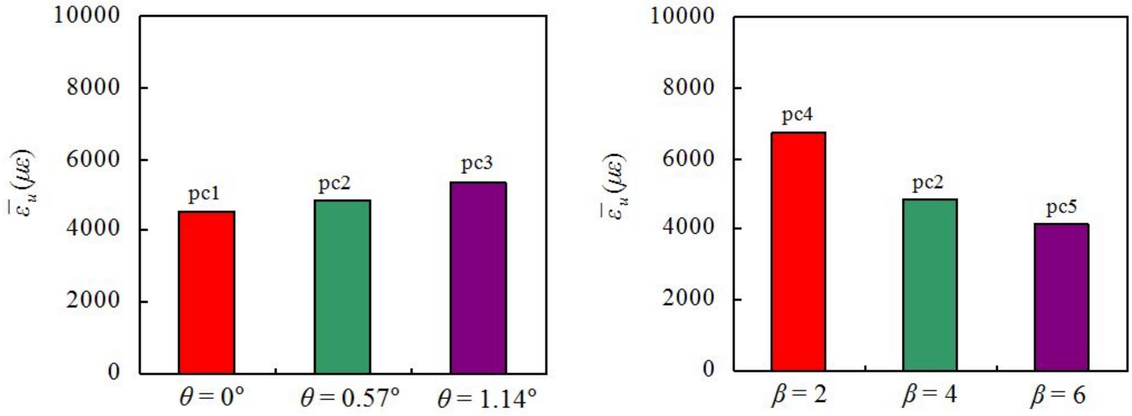

(a) Tapered angle (b) Partial compression area ratio

Fig. 18 Average strain ($\bar{\varepsilon}_u$) of specimens without top endplate

of β from 2 to 4 and to 6. It can be found that, the influence of θ and β on the average strain ($\bar{\varepsilon}_u$) of the tapered CFDST columns with top endplate is moderate, whereas the influence of t_a and the sandwich concrete on the average strains ($\bar{\varepsilon}_u$) of the tapered CFDST columns is significant.

For the tapered CFDST columns without top endplate, $\bar{\varepsilon}_u$ increases by 6.5% and 17.9%with the increase in θ from 0° to 0.57° and to 1.14°. $\bar{\varepsilon}_u$ decreases by 28.1% and 38.2% with the increases of β from 2 to 4 and to 6. It seems that the influence of θ on the average strain $\bar{\varepsilon}_u$ of the tapered CFDST columns without top endplate is minimal, whereas the influence of β on the average strain $\bar{\varepsilon}_u$ of the tapered CFDST columns without top endplate is significant.

Figs. 19(a) and (b) show the plotted average strain ($\bar{\varepsilon}_u$) versus tapered angle (θ) relations of the composite columns with and without top endplate. According to the measured data, empirical formulas of $\bar{\varepsilon}_u$ with respect to θ were given and shown in Fig. 19.

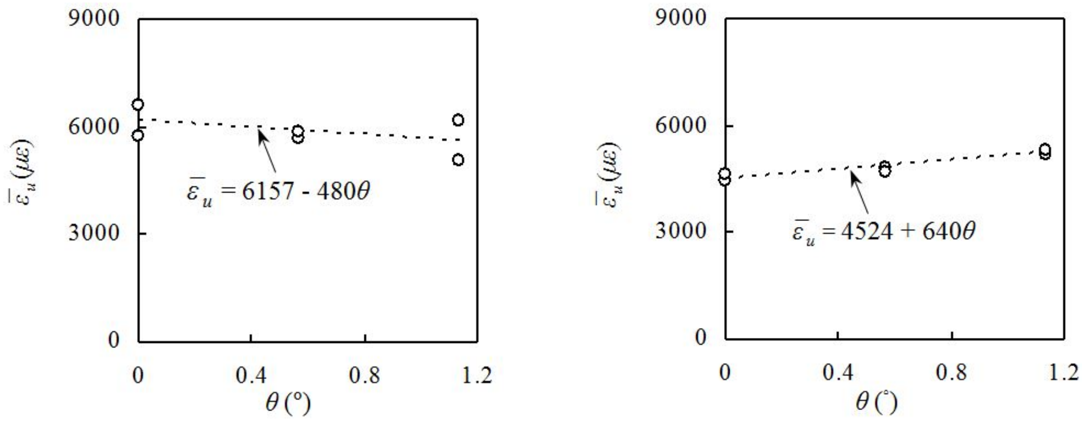

(a) With top endplate (b) Without top endplate

Fig. 19 Average strain ($\bar{\varepsilon}_u$) against tapered angle (θ) curves

3.3 Prediction of the bearing capacity

The bearing capacity of partially loaded CFDST sections (N_{up}) proposed by Yang *et al*. (2012) can be expressed as

$$N_{up} = K_{bc} N_{uf} \tag{4}$$

where, the bearing capacity factor (K_{bc}) is predicted using the following Eq. (5) for tapered CFDST with circular hollow section (outer) and circular hollow section (inner). N_{uf} is the predicted bearing capacity of the corresponding entirely loaded composite sections according to the formulae by Tao *et al*. (2004). Li *et al*. (2012) suggested that for tapered CFDST stub columns, the member strength can be referred to the cross-sectional strength which is dominated by the section with the minimum profile. Thus, for tapered CFDST columns, N_{uf} is the predicted bearing capacity of the top section, the profile of which is affected by the tapered angle (θ) and the height of the column (H) when the bottom section is the same.

Yang *et al*. (2012) conducted parametric analysis on K_{bc} and concluded that K_{bc} is significantly affected by those parameters χ, t_a and β. Based on regression of the test, K_{bc} for circular tapered CFDST can be expressed as

$$K_{bc} = \frac{\left(0.9 + 1.28\chi - 2.16\chi^2\right)\cdot\left(0.12t_a^{0.6} + 0.52\right)}{\left(0.28\beta^{0.5} + 0.44\right)} \tag{5}$$

where, χ is the hollow ratio which can be calculated as $d/(D\text{-}2t_o)$, t_a is the top endplate thickness, and β is the partial compression area ratio.

The bearing capacity of partially loaded tapered CFDST specimens in the present tests is predicted by using Eq. (4), and the comparison between the predicted and measured bearing

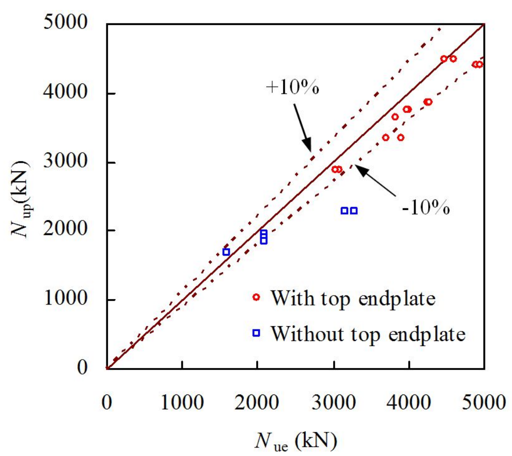

Fig. 20 Comparison between the predicted and measured bearing capacities

capacities is demonstrated in Fig. 20. It can be found that the predicted bearing capacities (N_{up}) are in good agreement with the measured results (N_{ue}). For the partially loaded tapered CFDST stub columns with top endplate, the average value of the N_{up}/N_{ue} is 0.927 and the standard deviation is 0.021, respectively and for partially loaded tapered CFDST stub columns without top endplate, the average value of N_{up}/N_{ue} is 0.899 and the standard deviation is 0.090, respectively.

4. Conclusions

This paper investigated the bearing capacity of tapered CFDST stub columns under axial partial compression. The following conclusions can be drawn within the scope of the current studies:

(1) Similar to CFDST stub columns under axial partial compression, the partially loaded tapered CFDST stub columns can develop stable load versus deformation response and exhibit a ductile behaviour.
(2) For partially loaded tapered CFDST stub columns with top endplate, the axial partial compression bearing capacity decreases with the increasing in tapered angle (θ) and partial compression area ratio (β), and increases with the increasing of top endplate thickness (t_a) and concrete infill.
(3) For partially loaded tapered CFDST stub columns without top endplate, the axial partial compression bearing capacity decreases with the increasing in tapered angle (θ) and partial compression area ratio (β).
(4) A simple model is proposed for predicting the bearing capacity of tapered CFDST stub columns under axial partial compression.

Acknowledgments

The research reported in the paper is part of Tsinghua Initiative Scientific Research Program (NO.2013Z02). The financial support is highly appreciated.

References

Dong, C.X. and Ho, J.C.M. (2012), "Uni-axial behaviour of normal-strength CFDST columns with external steel rings", *Steel Compos. Struct.*, *Int. J.*, **13**(6), 587-606.

Han, L.H., Liu, W. and Yang, Y.F. (2008), "Behaviour of concrete-filled steel tubular stub columns subjected to axially local compression", *J. Constr. Steel Res.*, **64**(4), 377-387.

Han, L.H., Ren, Q.X. and Li, W. (2010), "Tests on inclined, tapered and STS concrete-filled steel tubular (CFST) stub columns", *J. Constr. Steel Res.*, **66**(10), 1186-1195.

Han, L.H., Ren, Q.X. and Li, W. (2011), "Tests on stub stainless steel–concrete–carbon steel double-skin tubular (DST) columns", *J. Constr. Steel Res.*, **67**(3), 437-452.

Hu, H.T. and Su, F.C. (2011), "Nonlinear analysis of short concrete-filled double skin tube columns subjected to axial compressive forces", *Mar. Struct.*, **24**(4), 319-337.

Kim, J.K., Kwak, H.G. and Kwak, J.H. (2013), "Behavior of hybrid double skin concrete filled circular steel tube columns", *Steel Compos. Struct.*, *Int. J.*, **14**(2), 191-204.

Lam, D., Dai, X.H., Han, L.H., Ren, Q.X. and Li, W. (2012), "Behaviour of inclined, tapered and STS square CFST stub columns subjected to axial load", *Thin-Wall. Struct.*, **54**, 94-105.

Li, W., Ren, Q.X., Han, L.H. and Zhao, X.L. (2012), "Behaviour of tapered concrete-filled double skin steel tubular (CFDST) stub columns", *Thin-Wall. Struct.*, **57**, 37-48.
Li, W., Han, L.H., Ren, Q.X. and Zhao, X.L. (2013), "Behavior and calculation of tapered CFDST columns under eccentric compression", *J. Constr. Steel Res.*, **83**, 127-136.
Shimizu, M., Tatsumi, F., Ishikawa, T., Hattori, A. and Kawano, H. (2013), "Experimental study on ultimate strength of concrete filled double tubular steel with shear connector", *Int. J. Steel Struct.*, **13**(1), 49-54.
Tao, Z., Han, L.H. and Zhao, X.L. (2004), "Behaviour of concrete-filled double skin (CHS inner and CHS outer) steel tubular stub columns and beam-columns", *J. Constr. Steel Res.*, **60**(8), 1129-1258.
Uenaka, K., Kitoh, H. and Sonoda, K. (2008), "Concrete filled double skin tubular members subjected to bending", *Steel Compos. Struct.*, *Int. J.*, **8**(4), 297-312.
Yang, Y.F. and Han, L.H. (2012), "Concrete filled steel tube (CFST) columns subjected to concentrically partial compression", *Thin-Walled Struct.*, **50**(1), 147-156.
Yang, Y.F., Han, L.H. and Sun, B.H. (2012), "Experimental behaviour of partially loaded concrete filled double-skin steel tube (CFDST) sections", *J. Constr. Steel Res.*, **71**, 63-73.
Zhao, X.L. and Han, L.H. (2006), "Double skin composite construction", *Prog. Struct. Eng. Mater.*, **8**(3), 93-102.
Zhao, X.L., Grzebieta, R. and Elchalakani, M. (2002), "Tests of concrete-filled double skin CHS composite stub columns", *Steel Compos. Struct.*, *Int. J.*, **2**(2), 129-146.
Zhao, X.L., Tong, L.W. and Wang, X.Y. (2010), "CFDST stub columns subjected to large deformation axial loading", *Eng. Struct.*, **32**(3), 692-703.

CC

Nomenclature

A_c	:	Cross-sectional area of the sandwich concrete
A_p	:	Partial compression area
d	:	Outside diameter of the inner steel tube
d_r	:	Outside diameter of the ring bearing plate
D	:	Outside diameter of the outer steel tube
E_c	:	Elastic modulus of concrete
E_s	:	Elastic modulus of steel
f_{ck}	:	Characteristic strength of concrete ($f_{ck} = 0.67f_{cu}$ for normal strength concrete)
f_{cu}	:	Cube strength of concrete
f_y	:	Yield strength of steel
f_u	:	Ultimate strength of steel
H	:	Height of the stub column
K_{bc}	:	Bearing capacity factor
N	:	Axial load
N_{ue}	:	Measured bearing capacity
N_{uf}	:	Bearing capacity of entirely loaded composite sections
N_{up}	:	Predicted bearing capacity
N_{ur}	:	Average axial partial compression strength of the reference straight CFDST stub columns
SI	:	:Strength index
t	:	Wall thickness of the steel tube
t_a	:	top endplate thickness
t_i	:	Wall thickness of the inner steel tube
t_o	:	Wall thickness of the outer steel tube
t_r	:	Wall thickness of the ring bearing plate
γ_s	:	Poisson's ratio
β	:	Partial compression area ratio ($= A_c / A_p$)
Δ	:	Axial deformation
Δ_{ue}	:	Axial deformation corresponding to the bearing capacity
ε	:	Strain of steel
χ	:	Hollow ratio($= d / (D-2t_o)$)
θ	:	Tapered angle